

Antiphase dynamics in multimode semiconductor lasers with optical feedback

C. Masoller,^{1,2} M. S. Torre,³ and Paul Mandel⁴

¹*Departament de Física i Enginyeria Nuclear, Universitat Politècnica de Catalunya, Colom 11, E-08222 Terrassa, Spain*

²*Instituto de Física, Facultad de Ciencias, Universidad de la República, Igua 4225, Montevideo 11400, Uruguay*

³*Instituto de Física "Arroyo Seco," UNCPBA Pinto 399 (7000) Tandil, Argentina*

⁴*Optique Nonlinéaire Théorique, Université Libre de Bruxelles, Campus Plaine Code Postal 231, B-1050 Bruxelles, Belgium*

(Received 25 June 2004; revised manuscript received 27 September 2004; published 27 January 2005)

We study the dynamics of multimode semiconductor lasers with optical feedback. Our model takes into account explicitly spatial effects, which are included by considering spatial profiles for N longitudinal modes coupled to the space-dependent gain. We also consider the effect of carrier diffusion. We find that in the weak feedback regime the longitudinal modes display antiphase oscillations that lead to a nearly constant output intensity. This result is largely independent of the value of the diffusion coefficient. For larger feedback we observe in-phase fast oscillations at a frequency close to the relaxation oscillation frequency of the solitary laser. In these two regimes, the total output of the laser has the properties of a single-mode laser for nondispersive applications. We assess the validity of an existing approximation scheme that has dealt with spatial inhomogeneities by expanding the carrier density into a truncated hierarchy of moments. We demonstrate that this approximation is very good when the underlying carrier diffusion is fast, thus leading to a weakly developed carrier grating.

DOI: 10.1103/PhysRevA.71.013818

PACS number(s): 42.55.Px, 42.65.Sf

I. INTRODUCTION

Multi-longitudinal-mode laser dynamics is a difficult problem that has received increasing attention over the last ten years. In this paper, we focus on that topic for edge-emitting semiconductor lasers with optical feedback. These lasers are difficult to analyze because their size makes it extremely difficult to probe *in situ* the physics that takes place. It is only very recently that systematic experimental results on multi-longitudinal-mode edge-emitting semiconductor lasers have begun to be reported for more than two modes in the much simpler configuration without optical feedback [1].

Optical feedback adds an infinite number of dimensions to the phase space of the dynamical system and is expected to lead to an even more complex dynamics. Therefore the tendency has been to resort to phenomenological models to answer the inverse problem question: what physical mechanisms account for the observed laser output properties? For that purpose, two approaches have been mainly used. The first one does not presuppose the number of lasing modes and deals therefore with an electromagnetic field described by a partial differential equation. That field is coupled to the free-carrier density by means of either a diffusion equation [2,3] or the space average of the free-carrier density [4–6]. This approach does include some drastic approximations in the description of the semiconductor physics but retains most aspects of Maxwell's equations for the field. Its drawback is the heavy computational work that is required. The second approach is based on a modal expansion of the cavity field and on a moment expansion of the free-carrier density to generalize the Lang-Kobayashi single-mode model [7]. Two different ways to approximate the material diffusion equation have been used. One way is to approximate the free-carrier density by its space average, reducing the diffusion equation to an ordinary differential equation and leading to a set of $N+1$ equations if there are N lasing modes [8–12]. The other

way is to expand the free-carrier density in terms of the nonlinear gain function [13] as in solid-state laser rate equations [14]. This leads to a set of $2N$ equations for N lasing modes [15–17].

A significant difference between the two types of modal expansions is the underlying assumption about the free-carrier dynamics (also referred to as spatial hole burning or spatial grating). In the $N+1$ approach, it is assumed that diffusion washes out very fast any spatial inhomogeneity and that the free-carrier density may, to a very good approximation, be assumed to be a constant along the gain medium. On the contrary, the $2N$ approach assumes that the inhomogeneous mode structure of the Fabry-Pérot laser, which is proportional to $\sin^2(m\pi z/L)$ where m is an integer and L the cavity length, imprints a similar inhomogeneity on the free-carrier density even in the long-time limit.

Recently, a comparison between these two sets of modal rate equations has been carried out to assess their differences and relevance [18]. In particular, it was shown that antiphase dynamics is not compatible with the $N+1$ modal equations but appears naturally in the $2N$ modal equations. This is important because the existence of in-phase and antiphase dynamics was recently demonstrated indirectly [19] by comparing the power spectral density for total intensity with the incoherent sum of power spectral densities for individual modes and directly by ultrafast recording of the modal output power [1].

In the absence of a reliable experimental estimation of the lifetime of the spatial inhomogeneity of the free-carrier density, we propose in this paper to compare the two modal approaches described in this introduction with the model from which they both derive, namely, the set of N modal equations for the electromagnetic field coupled to the full diffusion equation for the free-carrier density. The optical feedback is taken into account as in the Lang-Kobayashi model, through a single delay term in the equations for the mode amplitudes. We find with the diffusion equation that

for weak feedback the modal intensities display antiphase oscillations that lead to a nearly constant output intensity, in good agreement with the predictions of the $2N$ model. Surprisingly, the antiphase oscillations occur in a wide range of values of the carrier diffusion coefficient. This indicates that weak diffusion is not a singular limit. More important, it suggests that even in the long-time limit and despite the assumption of a fast free-carrier dynamics, there remain traces of the spatial inhomogeneity induced by the mode gratings.

This paper is organized as follows. The model is described in Sec. II. Results of numerical simulations are presented in Secs. III and IV, and Sec. IV contains a summary and the conclusions.

II. THE MODEL

We begin by writing the optical field in the laser cavity as

$$E(z, t) = \sum_m [\phi_m(z)E(m, t) + \text{c.c.}], \quad (1)$$

where the $\phi_m(z)$ are in principle any set of functions that form an orthonormal basis. In practice, the usual choice is the modes of the empty lossless cavity, which for a Fabry-Pérot cavity of length L are given by $\phi_m = \sqrt{2} \sin(q_m z)$ where $q_m = \pm m\pi/L$, m being an integer and L the cavity length. The ϕ_m are normalized to unity: $(1/L) \int_0^L |\phi_m(z)|^2 dz = 1$. Next we define the slowly varying complex amplitudes as

$$E(m, t) = \mathcal{E}_m(t) \exp(i\omega_m t), \quad (2)$$

where $\omega_m = q_m c$.

The rate equations for a multimode laser which couple the modal complex amplitudes $\mathcal{E}_m(t)$ to the population inversion $F(z, t)$ are [16]

$$\frac{d\mathcal{E}_m(t)}{dt} = \frac{1+i\alpha}{2} [G_m(t) - \kappa_m] \mathcal{E}_m(t) + \eta_m \mathcal{E}_m(t - \tau) \exp(-i\omega_m \tau), \quad (3)$$

$$\begin{aligned} \frac{\partial F(z, t)}{\partial t} &= J(z) - \frac{F(z, t)}{\tau_s} - F(z, t) \sum_m |\phi_m(z) \mathcal{E}_m(t)|^2 \\ &+ D_z \frac{\partial^2 F(z, t)}{\partial z^2}. \end{aligned} \quad (4)$$

The G_m are the modal nonlinear gains,

$$G_m(t) = \frac{1}{L} \int_0^L |\phi_m(z)|^2 F(z, t) dz, \quad (5)$$

α is the linewidth enhancement factor, and κ_m is the field damping rate (or inverse photon lifetime). A delay term was included phenomenologically to account for weak external optical feedback [7]. η_m is the feedback strength into the m th mode and $\tau = 2L_{\text{ext}}/c$ is the delay time induced by the external cavity. In Eq. (4) $J(z)$ is the carrier injection current, τ_s is the carrier lifetime, and D_z is the longitudinal carrier diffusion coefficient.

We now derive the two approximate models described in the Introduction. Defining the spatial average of the carrier density as

$$\mathcal{N}(t) = \frac{1}{L} \int_0^L F(z, t) dz, \quad (6)$$

integrating Eq. (4) over z , and neglecting carrier diffusion gives

$$\frac{d\mathcal{N}}{dt} = \mathcal{J} - \frac{\mathcal{N}}{\tau_s} - \sum_m |\mathcal{E}_m|^2 G_m, \quad (7)$$

where $\mathcal{J} = (1/L) \int_0^L J(z) dz$. Equations (3) and (7), supplemented with a phenomenological expression for the modal gain G_m [which replaces Eq. (5)], constitute the set of $N+1$ rate equations that has been studied. In Refs. [8,11], the nonlinear gain is $G_m = \beta_m \mathcal{N}$ and β_m has a parabolic frequency dependence. In Ref. [9], the nonlinear gain is $G_m = \mathcal{N} \sum_k \beta_{mk} |E_k|^2$ where the β_{mk} have a Lorentzian dependence on the modal frequencies.

On the other hand, multiplying Eq. (4) by $|\phi_m(z)|^2$, integrating in z , and neglecting carrier diffusion gives

$$\frac{dG_m}{dt} = J_m - \frac{G_m}{\tau_s} - \sum_n \left[\int_0^L F |\phi_m(z)|^2 |\phi_n(z)|^2 dz \right] |\mathcal{E}_n|^2, \quad (8)$$

where $J_m = (1/L) \int_0^L J(z) |\phi_m(z)|^2 dz$. Approximating the last term in Eq. (8)

$$\int_0^L F(z, t) |\phi_m(z)|^2 |\phi_n(z)|^2 dz \sim \beta_{mn} G_m(t), \quad (9)$$

we obtain

$$\frac{dG_m}{dt} = J_m - \frac{G_m}{\tau_s} - G_m \sum_n \beta_{mn} |\mathcal{E}_n|^2. \quad (10)$$

Equations (3) and (10) constitute a set of $2N$ rate equations that are those studied in Ref. [15] and therefore formally equivalent to those studied in Refs. [16,17].

III. RESULTS

We present results of numerical simulations of Eqs. (3) and (4) with three longitudinal modes. We have also performed simulations with six or more longitudinal modes, finding similar results. The mode with $m=1$ has wave number $q_1 = 275\pi/L$, the mode with $m=2$ has $q_2 = 276\pi/L$, and the mode with $m=3$ has $q_3 = 277\pi/L$. We chose $L = 200 \mu\text{m}$ as the laser cavity length, which gives a wavelength for the central mode $\lambda_2 = 1450 \text{ nm}$. To focus on the effects induced only by the different spatial modal profiles, we assign to all modes the same cavity losses $\kappa_m = 1 \text{ ps}^{-1}$, feedback level, $\eta_m = \eta$, and feedback phase $\omega_m \tau = 0$ rad. Other parameters are $\alpha = 5$, $\tau_s = 1 \text{ ns}$, $\tau = 6 \text{ ns}$, $J(z) = 2000 (\sim 2J_{\text{th}})$, which means that J is uniform inside the active region. This choice for $J(z)$ is consistent with experimental values published [19,20], and to be published [21]. With these parameters, the relaxation oscillation frequency is about 5 GHz (the precise value depends on the diffusion coefficient). The spatial integration step was $dz = 0.02 \mu\text{m}$ and the time integration step was dt

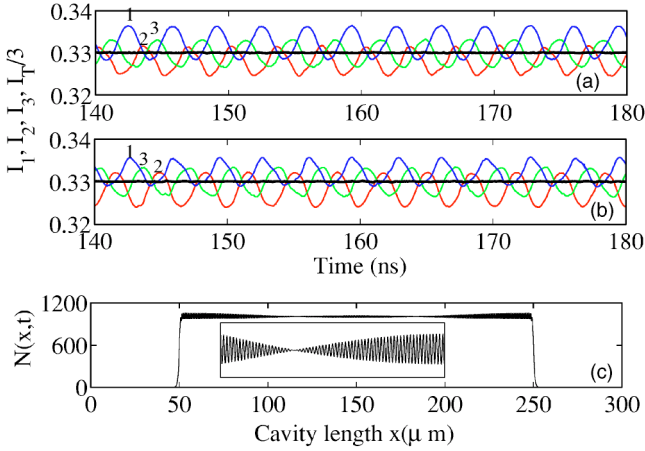


FIG. 1. (a) Modal intensities (thin lines) and total intensity divided by 3 (thick line) for $D_z=0.3 \mu\text{m}^2/\text{ns}$ and $\eta=0.25 \text{ ns}^{-1}$. (b) Parameters as in (a) but different initial conditions. For the initial conditions, the modal amplitudes are at the noise level. Thus, to vary the initial conditions we choose a different realization of the noise. (c) Carrier grating at $t=180 \text{ ns}$. The carrier grating is the same for the oscillations displayed in (a) and (b). The inset displays details of the spatial grating between $x=50$ and $150 \mu\text{m}$.

$=0.01 \text{ ps}$. For the initial conditions, the modal amplitudes are at the noise level and the excess carrier density is zero. The feedback level η and the diffusion coefficient D_z are the free parameters of our study.

Figure 1 displays results for $D_z=0.3 \mu\text{m}^2/\text{ns}$ and $\eta=0.25 \text{ ns}^{-1}$. The modal intensities $I_m=|\mathcal{E}_m|^2$ (thin lines) and $I_T/3=(1/3)\sum_m I_m$ (thick line) are plotted as a function of time. A regime of antiphase dynamics develops after the transients. In this regime the three longitudinal modes oscillate with a period $P\sim 3.3 \text{ ns}$ and each mode is phase shifted by nearly $P/3$. As a result, the total intensity is nearly constant. Varying the initial conditions changes the phase relations among the three modes. In Fig. 1(a) we observe the sequence 1-2-3 where the $m=2$ mode has a maximum after the $m=1$ mode and before the $m=3$ mode. Figure 1(b) displays a regime obtained with the same parameters as in Fig. 1(a) but a different initial condition. Here the sequence 1-3-2 is observed, as the $m=3$ mode has a maximum after the $m=1$ mode and before the $m=2$ mode. Both sequences correspond to the same carrier grating, which is displayed in Fig. 1(c).

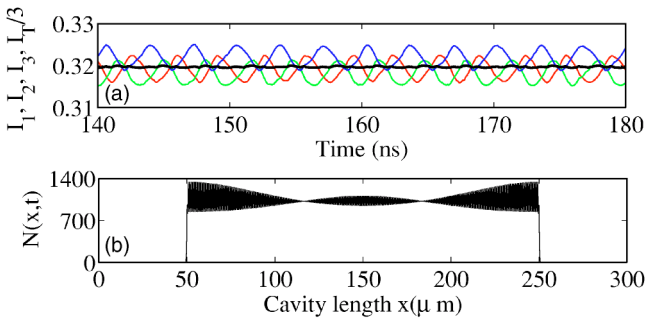


FIG. 2. (a) Modal intensities and total intensity divided by 3. (b) Carrier grating at $t=180 \text{ ns}$. $D_z=0.03 \mu\text{m}^2/\text{ns}$. Graphic conventions and all other parameters as in Fig. 1.

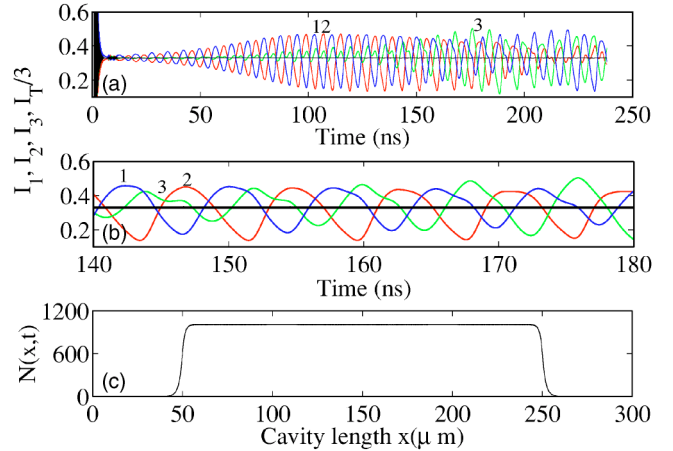


FIG. 3. (a) Modal intensities and total intensity divided by 3 for $D_z=3.0 \mu\text{m}^2/\text{ns}$; all other parameters as in Fig. 1. (b) Magnification of a short time interval of (a). It can be observed that the oscillations of the modal intensities follow the pattern 1-3-2 while the modal envelopes follow the pattern 1-2-3. (c) Carrier grating at $t=180 \text{ ns}$.

Decreasing D_z to $0.03 \mu\text{m}^2/\text{ns}$ (Fig. 2) still produces a self-structured dynamics. It can be observed that due to the slower carrier diffusion there is a more pronounced hole-burning effect, which leads to a more developed carrier grating.

Increasing D_z to $3 \mu\text{m}^2/\text{ns}$ (Fig. 3) leads to a regime in which the total output is still constant but there is a large amplification of the modulation amplitude of $I_1, I_2,$ and I_3 , which also displays antiphase dynamics. With three modes there are only two topologically different modal sequences of antiphase dynamics: 1-2-3 and 1-3-2. While the modal envelopes follow the sequence 1-2-3 [Fig. 3(a)], the fast pulses display antiphase 1-3-2 [Fig. 3(b)]. Figure 3(c) shows that, due to fast carrier diffusion, there is only a weakly developed carrier grating.

Figure 4 displays results for a larger number of modes ($N=7$). A complex antiphase regime resulting in a complete compensation of the modal intensity oscillations in the total output power is observed [Fig. 4(a)]. The carrier grating [Fig. 4(b)] exhibits fast oscillations (due to mode-mode beating) which are modulated by a slow envelope, which is related to the number of operating modes (with seven longitudinal modes there are six “nodes”).

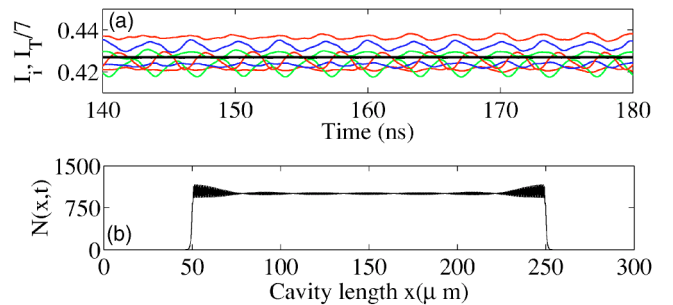


FIG. 4. As in Fig. 1 but with seven longitudinal modes. $J=4000$; all other parameters as in Fig. 1. (a) Modal intensities and total intensity divided by 7; (b) carrier grating at $t=180 \text{ ns}$.

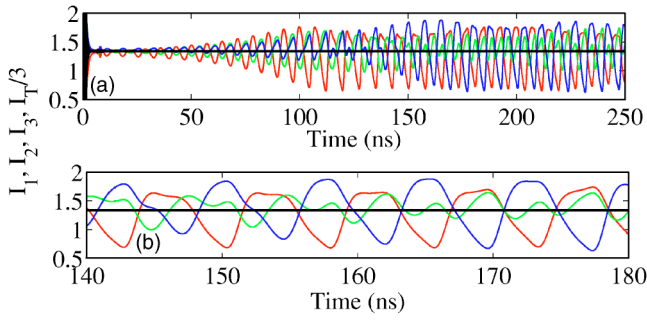


FIG. 5. (a) Modal intensities and total intensity divided by 3, obtained simulating Eqs. (3) and (10) (formally equivalent to that proposed in Ref. [15]) with parameters $J_m=5000$, $\beta_{mn}=0.996$; other parameters as Fig. 1. (b) Magnification of a short time interval of (a).

The observed dynamics is in agreement with the antiphase dynamics predicted from a normal form analysis [14] and for a semiconductor laser with external feedback [15] in the framework of the model of Eqs. (3) and (10). We have made simulations of that model, shown in Fig. 5, to demonstrate the good qualitative agreement between the two models. We do not present simulations based on the $N+1$ equations as it was recently shown [18] that this model exhibits, in the absence of noise, only steady-state or in-phase dynamics, while in the presence of noise, it exhibits only out-of-phase oscillations but no antiphase states such as the 1-2-3 and the 1-3-2 oscillations displayed Figs. 1–3.

The above results show that for weak optical feedback there is a compensation of the modal oscillations in the total output intensity that is independent of the value of the diffusion coefficient in the range studied. This result implies, in that range of diffusion coefficients, that the output of the laser can be considered as constant in time, providing it is not used in a dispersive setup. For larger optical feedback this compensation is destroyed, and the feedback strength for which this transition occurs depends on the diffusion coefficient.

For weak carrier diffusion ($D_z=0.3 \mu\text{m}^2/\text{ns}$) and $\eta=1.0 \text{ ns}^{-1}$, the modal intensities oscillate in phase. Figure 6(a) shows the total output intensity and Fig. 6(b) the modal intensities (for clarity the intensities of the $m=1$ and 3 modes are shifted vertically by $+0.1$ and -0.1 , respectively). It can be observed that the modal intensities exhibit fast pulses at a frequency close to the relaxation oscillation frequency, and a modulation of the envelope at a frequency close to the external cavity frequency. As a result, the total output becomes deeply modulated at the external cavity frequency. The time trace shown in Fig. 6(a) looks remarkably similar to solutions of the single-mode Lang-Kobayashi equations [22] in similar conditions.

For larger feedback strength [$\eta=2.0 \text{ ns}^{-1}$, Figs. 6(c) and 6(d)] the dynamics becomes increasingly chaotic. The modal intensities are still in phase (extrema of the same kind occur at the same time for all modes) but with different amplitudes.

For larger carrier diffusion ($D_z=3.0 \mu\text{m}^2/\text{ns}$) and $\eta=1.0 \text{ ns}^{-1}$, it can be observed in Figs. 7(a) and 7(b) that the modal intensities still oscillate in antiphase, resulting in a

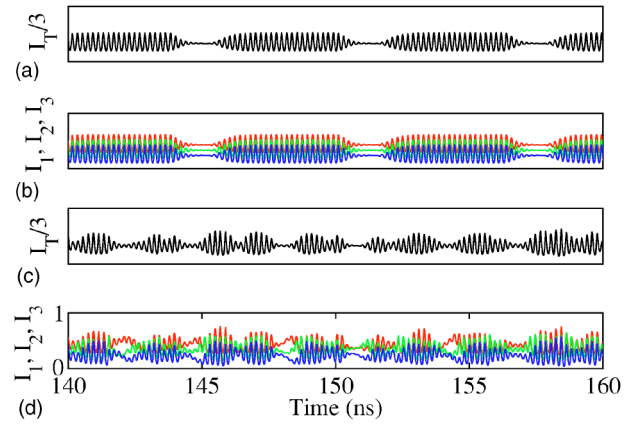


FIG. 6. Dynamics for larger optical feedback and slow diffusion. (a),(b) $\eta=1.0 \text{ ns}^{-1}$; (c),(d) $\eta=2.0 \text{ ns}^{-1}$; all other parameters as in Fig. 1. (a) and (c) display the total intensity divided by 3; (b) and (d) display the modal intensities (for clarity the modal intensities of modes 1 and 3 have been shifted vertically $+0.1$ and -0.1 , respectively).

constant total output power. For larger optical feedback [$\eta=2.0 \text{ ns}^{-1}$, Figs. 7(c) and 7(d)] the modal intensities are again in phase (extrema of the same kind occur at the same time for all modes) but with different amplitudes.

To further characterize this chaotic dynamics we employ the technique proposed in [19] and used in [18]. Let $P(I_T, f)$ and $P(I_i, f)$ be the power spectral densities of the total output power and of the i th mode, respectively, at frequency f . If the modes are in perfect antiphase at frequency f , then $P(I_T, f) = 0$; if they are in perfect inphase at frequency f , then $P(I_T, f) = [\sum \sqrt{P(I_i, f)}]^2$; and if they are in partial antiphase, then $\sum P(I_i, f) > P(I_T, f) > 0$ at frequency f . Figures 8(a) and 8(b) display $P(I_T, f)$ and $\sum P(I_i, f)$ for the parameters of Figs. 6(c), 6(d), 7(c), and 7(d), respectively. It can be observed that the modes exhibit partial antiphase dynamics at low frequencies, and in-phase dynamics at high frequencies. This behavior agrees well with experimental observations [19] and the theoretical analysis of Eqs. (3) and (10) in Ref. [18].

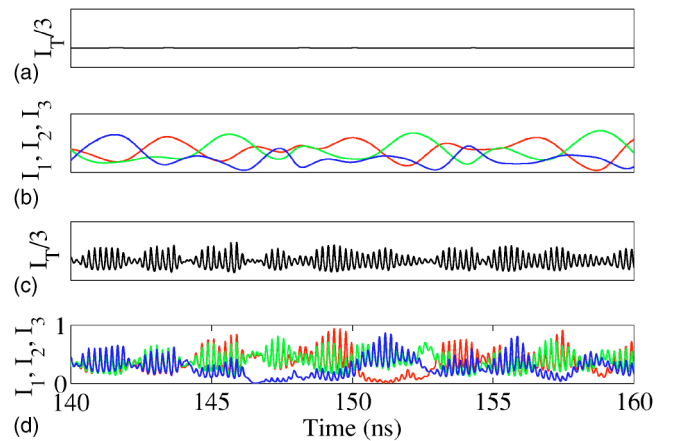


FIG. 7. Dynamics for larger optical feedback and fast diffusion. (a),(b) $\eta=1.0 \text{ ns}^{-1}$; (c),(d) $\eta=2.0 \text{ ns}^{-1}$; all other parameters as in Fig. 3. (a) and (c) display the total intensity divided by 3; (b) and (d) display the modal intensities.

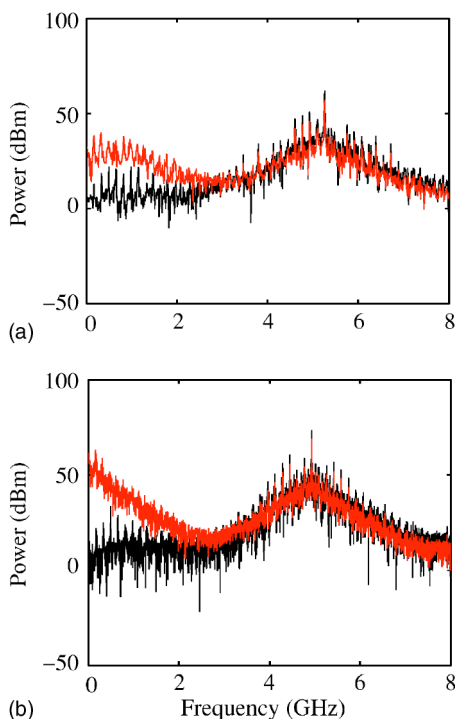


FIG. 8. (Color online) Power spectral densities: $P(I_T, f)$ [gray (red) line] and $\Sigma P(I_T, f)$ (black line). (a) Parameters as in Figs. 6(c) and 6(d). (b) Parameters as in Figs. 7(c) and 7(d). Antiphase dynamics is observed at low frequencies.

IV. CONCLUSIONS

We studied the dynamics of a multi-longitudinal-mode semiconductor laser with weak optical feedback based on an extension of the single-mode Lang-Kobayashi model. We focus on effects induced by spatial inhomogeneities. Our model includes spatial profiles for the longitudinal modes

and for the carrier density in the laser cavity. The carrier density verifies a diffusion equation. We have shown that for low enough feedback there is antiphase dynamics, resulting in a compensation of the modal oscillations in the total output intensity, which is independent of the carrier diffusion. As the feedback increases the relaxation oscillation frequency becomes undamped, and we observe inphased modal oscillations. For larger feedback the dynamics becomes chaotic, and modal intensities remain in phase but with different chaotic amplitudes.

The coherence of the time-dependent modal intensities, originating from the global coupling of the modes (all modes interact with the same gain medium), results in a practically constant output intensity. This explains why a number of features of multimode lasers could be successfully explained with single-mode models.

We have compared the predictions of our model (which includes explicitly the carrier density spatial profile and a carrier diffusion term) with those of the model represented by Eqs. (3) and (10), which approximates the carrier inhomogeneities by a set of finite nonlinear modal gains. We found that the agreement is particularly good in the limit of large diffusion, where the grating is relatively small due to the carrier diffusion; as expected, the agreement is less good in the weak diffusion limit, where approximating the grating by a finite set of moments is less valid.

ACKNOWLEDGMENTS

C.M. was supported in part by Proyecto de Desarrollo de Ciencias Basicas (PEDECIBA) and Comision Sectorial de Investigacion Cientifica (Uruguay). M.S.T. was supported in part by a grant from Secretaria de Ciencia y Técnica (UNCPBA-Argentina). P. M. was supported by the Fonds National de la Recherche Scientifique and the Interuniversity Attraction Poles Program—Belgian Science Policy.

-
- [1] A. M. Yacomotti *et al.*, Phys. Rev. A **69**, 053816 (2004).
 [2] P. Ru, J. V. Moloney, and R. Indik, Phys. Rev. A **50**, 831 (1994).
 [3] J. F. Mercier and J. V. Moloney, Phys. Rev. E **66**, 036221 (2002).
 [4] M. Homar, J. V. Moloney, and M. San Miguel, IEEE J. Quantum Electron. **32**, 553 (1996).
 [5] G. Huyet *et al.*, Phys. Rev. A **60**, 1534 (1999).
 [6] C. Serrat, S. Prins, and R. Vilaseca, Phys. Rev. A **68**, 053804 (2003).
 [7] R. Lang and K. Kobayashi, IEEE J. Quantum Electron. **16**, 347 (1980).
 [8] J. Mørk, B. Tromborg, and P. L. Christiansen, IEEE J. Quantum Electron. **24**, 123 (1988).
 [9] D. W. Sukow *et al.*, Phys. Rev. A **60**, 667 (1999).
 [10] D. Yu, L. Wallace, R. G. Harrison, and A. Gavrielides, Opt. Commun. **195**, 249 (2001).
 [11] F. Rogister, P. Mégret, O. Deparis, and M. Blondel, Phys. Rev. A **62**, 061803(R) (2000).
 [12] J. M. Buldu *et al.*, J. Opt. B: Quantum Semiclassical Opt. **4**, 415 (2002).
 [13] P. Mandel, Eur. Phys. J. D **8**, 431 (2000).
 [14] A. G. Vladimirov, E. A. Viktorov, and P. Mandel, Phys. Rev. E **60**, 1616 (1999).
 [15] E. A. Viktorov and P. Mandel, Phys. Rev. Lett. **85**, 3157 (2000).
 [16] T. W. Carr, D. Pieroux, and P. Mandel, Phys. Rev. A **63**, 033817 (2001).
 [17] P. Mandel *et al.*, Physica A **327**, 129 (2003).
 [18] I. Koryukin and P. Mandel, Phys. Rev. A **70**, 053819 (2004).
 [19] A. Uchida, Y. Liu, I. Fischer, P. Davis, and T. Aida, Phys. Rev. A **64**, 023801 (2001).
 [20] I. Fischer, Y. Liu, and P. Davis, Phys. Rev. A **62**, 011801(R) (2000).
 [21] M. W. Lee, J. Paul, C. Masoller, and K. A. Shore (unpublished).
 [22] C. Masoller and N. B. Abraham, Phys. Rev. A **57**, 1313 (1998).